Applied Nanoscience (2018) 8:11–18
https://doi.org/10.1007/s13204-018-0647-6

ORIGINAL ARTICLE

Effect of heating on the structural and optical properties of TiO_2 nanoparticles: antibacterial activity

Sirajul Haq[1] · Wajid Rehman[1] · Muhammad Waseem[2] · Rehan Javed[2] · Mahfooz-ur-Rehman[1] · Muhammad Shahid[3]

Received: 30 June 2017 / Accepted: 22 November 2017 / Published online: 3 February 2018

Abstract

TiO_2 nanoparticles were synthesized at room temperature by chemical precipitation method and were then heated at 120, 300, 600 and 900 °C temperatures. The phase transition and crystallite size variation were determined by X-rays diffraction (XRD) analysis. The surface area, pore volume and pore size were measured using Brunauer–Emmet–Teller (BET) and Barrett–Joyner–Halenda (BJH) methods. The optical activity of heat treated and non-heat treated samples were carried out by diffuse reflectance (DR) spectroscopy. Four different methods were used to calculate band gap energy. The results obtained from thermogravimetric and differential thermal gravimetric (TG/TDG) analyses and Fourier transform infra-red (FTIR) spectroscopy agreed with each other. Agar well diffusion method has been applied to explore the antibacterial activity of nanoparticles against different bacterial strains such as *Bacillus subtilis*, *Staphylococcus Aureus, Escherichia coli* and *Pseudomonas Aeruginosa*. It was observed that TiO_2 nanoparticles heated at 120 °C displayed maximum antibacterial activity while those heated at higher temperature showed no activity against the examined bacteria.

Keywords Antibacterial activity · Heating · Phase transition · Rutile. Surface area

Introduction

TiO_2 is one of the oxides that have attracted the attention of many researchers due to wide range of applications. It has three main polymorphs namely anatase, rutile and brookite. Out of these, anatase possess excellent biological, chemical and physical natural remediation (Zhao et al. 2007; Wang et al. 1997; Paunesku et al. 2003). The biological, chemical and physical properties are prominently influenced by the crystal phase, geometry and particle size (Yang et al. 2008, 2009; Han et al. 2009). Because of its heat stability, low cost and biocompatibility, they are widely used as cosmetic and skin care especially in sun block cream, pigment, sensors and photo catalyst (Dai et al. 2009; Joo et al. 2005; Li and Wang 2003; Arami et al. 2007; Sun et al. 2011).

✉ Muhammad Waseem
waseem_atd@yahoo.com

[1] Department of Chemistry, Hazara University, 21300 Mansehra, Pakistan

[2] Department of Physics, COMSATS Institute of Information Technology, Islamabad, Pakistan

[3] School of Chemical and Materials Engineering, National University of Sciences and Technology, Islamabad, Pakistan

Chemical precipitation method is widely used as compared to the other methods, reported for the synthesis of TiO_2 nanoparticles (Samuneva et al. 1993; Mazdiyasni et al. 1965; Cheng et al. 1995; Durand et al. 1995). The heating is an important technique which controls biological, chemical and physical properties of nanoparticles. The heating process affects the crystal phase and particle size which alter the biological, chemical and physical properties of the nanoparticles.

Microbial resistance to antibiotics is a world-wide problem in humans and animals due to the extensive use of antibiotic (Van den Bogaard and Stobberingh 2000). That is why the demand of new antimicrobial mechanism and new drug increase with the passage of time. The development of nanotechnology has explored different nanoparticles for medical applications. Along with many other applications, nanoparticles have useful and unique therapeutic use (Gao et al. 2004). In the same way, TiO_2 nanoparticles were previously used as antimicrobial agent against various type of microbes (Verdier et al. 2014).

The present study is aimed to focus on the synthesis of TiO_2 nanoparticles and to study the effect of heating on the phase transition, particles size, surface area, pore volume and band gap energy. The antibacterial activity of the heated

and unheated samples was one of the main objectives of the proposed work.

Results and discussion

Characterization TiO_2 nanoparticles

The XRD pattern of TiO_2 nanoparticles heated at different temperature is shown in Fig. 1. The XRD patterns of TiO_2 nanoparticles dried at 120 °C showed characteristic peaks at 2θ value 25.29° and for the samples dried at 300 and 600 °C were at 32.54° with hkl plane (101). These diffraction peaks were matched with JCPDS (joint committee on powder diffraction standards) card numbers 00-004-0477, 01-071-1168 and 01-071-1167 confirming the anatase phase with tetragonal geometry. However, the TiO_2 nanoparticles heated at 900 °C exhibit only the rutile phase with tetragonal geometry. This phase was confirmed by the appearance new diffraction peaks with hkl planes at 37.70° (110), 58.75° (220) and 71.01° (311) matched with JCPDS card no 01-076-1938. The phase transition temperature from anatase to rutile was observed above 600 °C (Kim and Hahn 2001; Kumar et al. 1993).

The crystallite size and lattice strain were calculated at different heating temperature using Debye-Scherer's equation and the extracted data was summarized in Table 1 (Chen et al. 2003). This table shows that heating the sample till

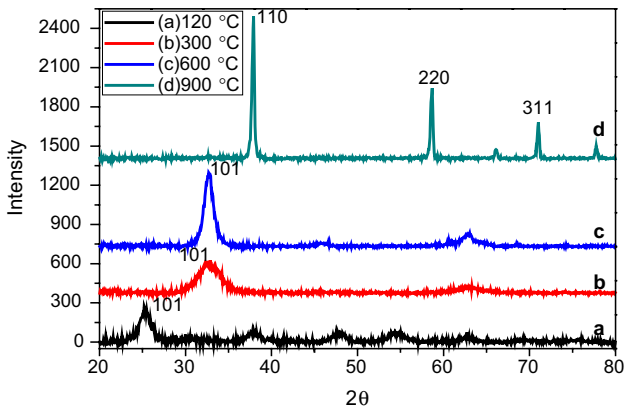

Fig. 1 XRD patterns of TiO_2 nanoparticles heat treated at various temperatures

300 °C temperature showed no major effect on the crystallite size, however, further increase in temperature to 600 °C and then at 900 °C have shown a profound effect on the crystallite size. The increase in crystallite size with increasing heating temperature can be attributed to thermally promoted crystallite growth (West 1986). The table further shows that by increasing the crystallite size, lattice strain decreases which infers that rutile phase is more stable than anatase. This may be because more particles are present at the crystal surface (having small crystallite size) and contribute to defects resulting higher lattice strain. When the samples were heated at higher temperatures, the crystallite size increases with the decrease in the number of surface particles. The crystal structure tends to be more perfect and, therefore, lattice strain decreases gradually (Wang et al. 2003). The dislocation density (δ) which represent the defect in the nanostructure is calculated by the formula ($\delta = 1/D^2$). Where D is the grain size that can be calculated using Sherrer's equation. The dislocation density decreases with increasing heating temperature. This may be due to increase in the crystallite size of TiO_2, the rearrangements and the crystal growth (Gaber et al. 2014).

Table 2 represents the surface area of heated TiO_2 nanoparticles calculated by different approaches such as single and multipoint BET, Langmuir, t-plot external surface area and BJH methods whereas Table 3 summarizes the pore size and pore volume. As can be seen from Table 2 and 3, pore volume, pore size and surface area decrease with increasing the heating temperature. A little variation can be seen when the samples were heated at 120 and 300 °C. However, when the heating temperature was increased further, a significant decrease in these parameters was detected. The decrease in the pore volume and surface area with heating temperature may be due to the collapse of crystal structure. The increase in pore size till 300 °C is due to the loss of water from the sample as has also been supported by TGA analysis. Further increase in heating temperature causes a decrease in pore size may be due to growth and rearrangement of TiO_2 crystallites. Similar increasing–decreasing pattern of pore size with heating temperature was also reported elsewhere (Yu et al. 2003).

Figure 2 displays the TG/DTG of heated at 120, 300, 600 and 900 °C temperatures. The TGA curve for sample "a" shows 13.345% weight loss due to the elimination of absorbed moisture in the range of 30–400 °C supported by

Table 1 Crystallite size, lattice strain and dislocation density of TiO_2 nanoparticles

Crystal Phase	TiO_2 (120 °C) Anatase	TiO_2 (300 °C)	TiO_2 (600 °C)	TiO_2 (900 °C) Rutile
Crystallite size (nm)	8.01	13	22.26	69.43
Lattice strain (%)	1. 94	1.04	0.45	0.15
Dislocation density $(nm)^{-2}$	1.55×10^{-2}	5×10^{-3}	2×10^{-3}	2×10^{-4}

Table 2 Surface area (m^2/g) of TiO_2 nanoparticles heated at various temperature

Temperature (°C)	Single point BET	BET	Langmuir	t-Plot (ext.)	BJH adsorption cumulative
120	151.07	156.95	231.93	174.75	180.28
300	149.21	154.68	228.42	173.69	175.19
600	56.27	57.72	84.31	58.90	37.07
900	03.81	4.04	06.06	04.68	03.03

Table 3 Pore volume (cm^3/g) and pore size (Å) of TiO_2 nanoparticles heated at various temperature

Temperature (°C)	Pore volume (cm^3/g)		Pore size (Å)	
	Single point BET (10^{-3})	BJH adsorption cumulative (10^{-3})	Adsorption average pore width (4 V/A by BET)	BJH cumulative
120	71.53	95.63	18.23	21.23
300	70.66	95.06	18.27	21.70
600	26.65	19.16	18.46	20.67
900	01.80	1.54	17.85	20.34

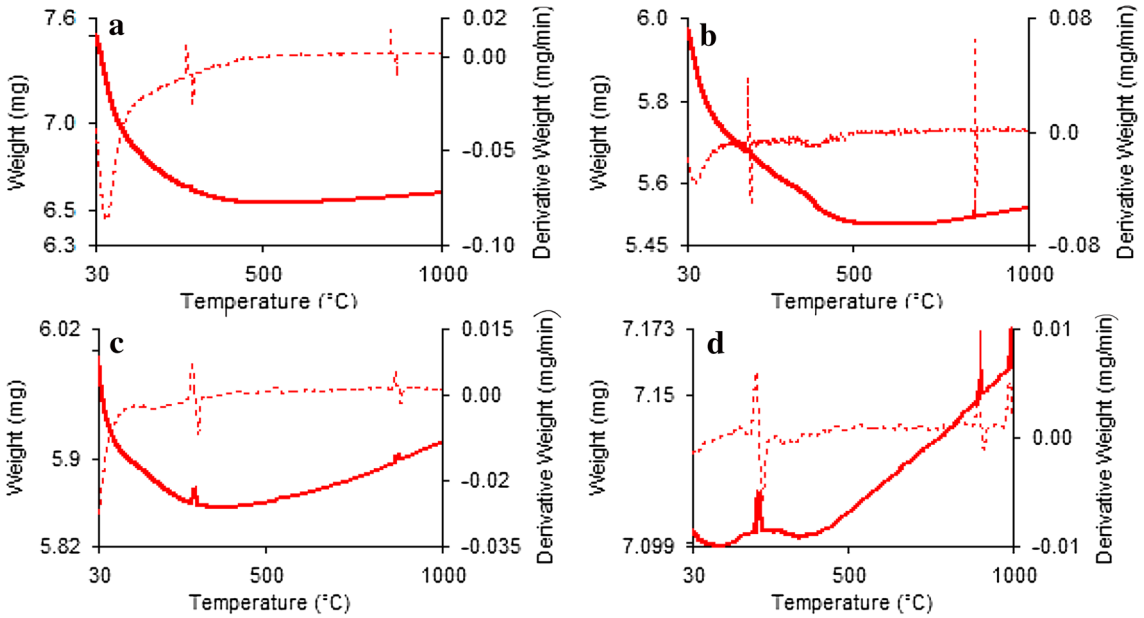

Fig. 2 TG/DTG curves of samples at 120 °C (**a**), 300 °C (**b**), 600 °C (**c**) and 900 °C (**d**)

the endothermic peaks in DTG curve between 30–50 °C and 285 °C. The loss of chemisorbed water was supported by the appearance of a broad endothermic peak around 390–410 °C, while an endothermic peak at 860 °C can be associated to the condensation of $Ti(OH)_2$ to TiO_2 (Farrukh et al. 2012). The other two exothermic peaks at 270 and 845 °C may be due to the decomposition of organic molecules and completion of any reaction resulting in weight increase. The weight loss for sample b was noted about 6.94% of total weight taken. The temperature profile for surface and chemisorbed water was found between 30 and 400 °C. However, after 800 °C, 0.03 mg weight gain was detected and is supported by DTG measurements. The exothermic peaks at 270 and 830 °C are due to the breakdown of hydrocarbon moieties resulting an increased weight which is because of phase transformation (Kayani et al. 2015). The TGA analysis for sample "c" displays a weight gain 0.05 mg beyond 500 °C along with the weight loss in the range 30–400 °C associated to the dehydration of water molecules. This sample also shows sharp endothermic peaks at 40, 120 and 550 °C associated to the weight loss related to removal of moisture contents, physically and chemically absorbed water, respectively. Sample

"d" shows 0.058 mg of increase in weight above 400 °C. The endothermic peaks at 230 and 920 °C are related to the loss of absorbed water and condensation of $Ti(OH)_2$ to TiO_2 whereas the exothermic peaks for sample "c" at 280 and 870 °C and for sample "d" at 185, 200, 900 and 990 °C are attributed to the decomposition of organic moieties, phase transformation and the rearrangement of particles after the removal of either impurities or completion of any reaction that resulted an increase in weight gain (Kayani et al. 2015).

The FTIR spectra of TiO_2 nanoparticles heated at various temperature are given in Fig. 3. The TiO_2 samples show main peaks in the range 520–1357 cm^{-1}, the peak at 520 cm^{-1} assigned to Ti–O stretching mode whereas the absorption band positioned at 1061 cm^{-1} was attributed to Ti–O–Ti (Waseem et al. 2011). The band centered at 1251 cm^{-1} was associated to O–Ti–O vibrations. It was noted that the intensity of band associated to OH vibration decreases with increase in heating temperature which may be due to the condensation of $Ti(OH)_2$ to TiO_2 (Yu et al. 2003). The intensities of bands linked to Ti–O, Ti–O–Ti and O–Ti–O were increased with temperature which might be due to the presence of impurities responsible for promoting the Ti–O and Ti–O–Ti network resulting the crystallization of TiO_2.

The UV–Vis reflectance spectra of TiO_2 nanoparticles heated at different temperature are given in Fig. 4. The wavelength of transmittance edge was determined by extrapolating the sharply rising part and horizontal part of the UV–Vis curves, showing the transmittance edge (as wavelength) according to pervious finding (Uddin et al. 2012). The transmittance edge determination and band gap energy calculation was on the basis of transmittance edge as shown in Fig. 4a. To find out the optical band gap as given in Fig. 4b, the reflectance values were converted into absorbance by applying Kubelka Mung function and modified Kubelka Mung function. The optical transition of semiconductor materials takes place by direct and indirect transition. The direct and indirect band gaps were calculated from the absorbance data as plotted in Fig. 4c and 4d. The transmittance edge and corresponding band gaps calculated by different methods are summarized in Table 4. A significant decrease in transmittance below 400 nm was seen due to the absorption of light causing the excitation of electrons from the valance shell to conduction band.

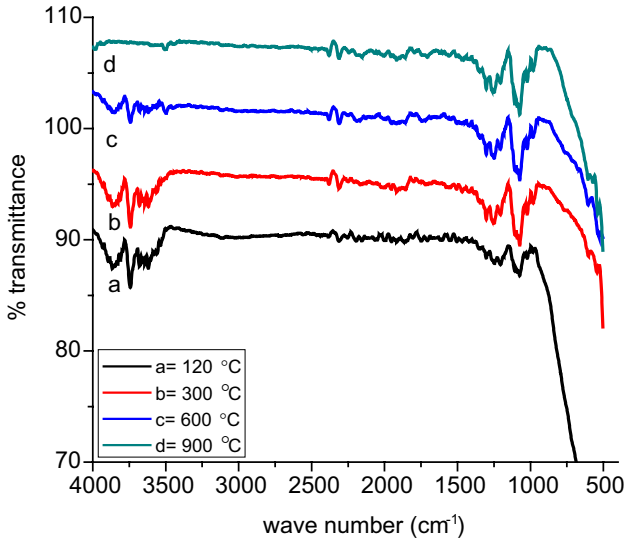

Fig. 3 FTIR spectra of TiO_2 nanoparticles heated at different temperatures

The decrease in % transmittance value may due to the increase in crystallite size, phase structure and surface roughness. The band gap energies calculated by different methods show a similar decreasing pattern with increasing the heating temperature (Table 4). The decrease in band gap energies at higher temperatures might be due to the increased energy of the electron of TiO_2. Due to the reduction of carrier density, caused by the removal of oxygen vacancies at high heating temperature, a decrease in band gap may be attributed to Burstein-Mott shift (Nagarani 2013).

Antibacterial activity

TiO_2 nanoparticles heated at different temperature were tested against *Staphylococcus aureus*, *Bacillus subtilis*, *Escherichia coli* and *Pseudomonas aeruginosa* to see the effect of heating on antibacterial activity using agar well diffusion method as shown in Fig. 5.

For antibacterial analysis, four different suspension of TiO_2 nanoparticles was prepared having different particle size. The activity of TiO_2 nanoparticles was more against *E. coli* than other examined bacterial species as suggested in the previous study (Prasad et al. 2011). The suspension TiO_2 nanoparticles having small particle size was more active against the examined bacteria then the large particles as shown in Fig. 5 and the inhibition zone value (in mm) are given in Table 5. As particles size increase with increasing heating temperature, the activity of TiO_2 nanoparticles against bacterial cells get decreased (Durucan and Akkopru 2010). The TiO_2 nanoparticles heated at 600 °C was less active while those heated at 900 °C had no activity against the test bacterial species. The possible explanation is that a single isolate colony of bacterial species can accommodate a large number of small TiO_2 particles as compared to large one resulting different antibacterial activity of the suspensions as reported in the previous study (Padmavathy and Vijayaraghavan 2008).

Keeping in view the crystallite size and surface area, the smaller particle with larger surface area exhibit high activity against all the examined bacterial species. This

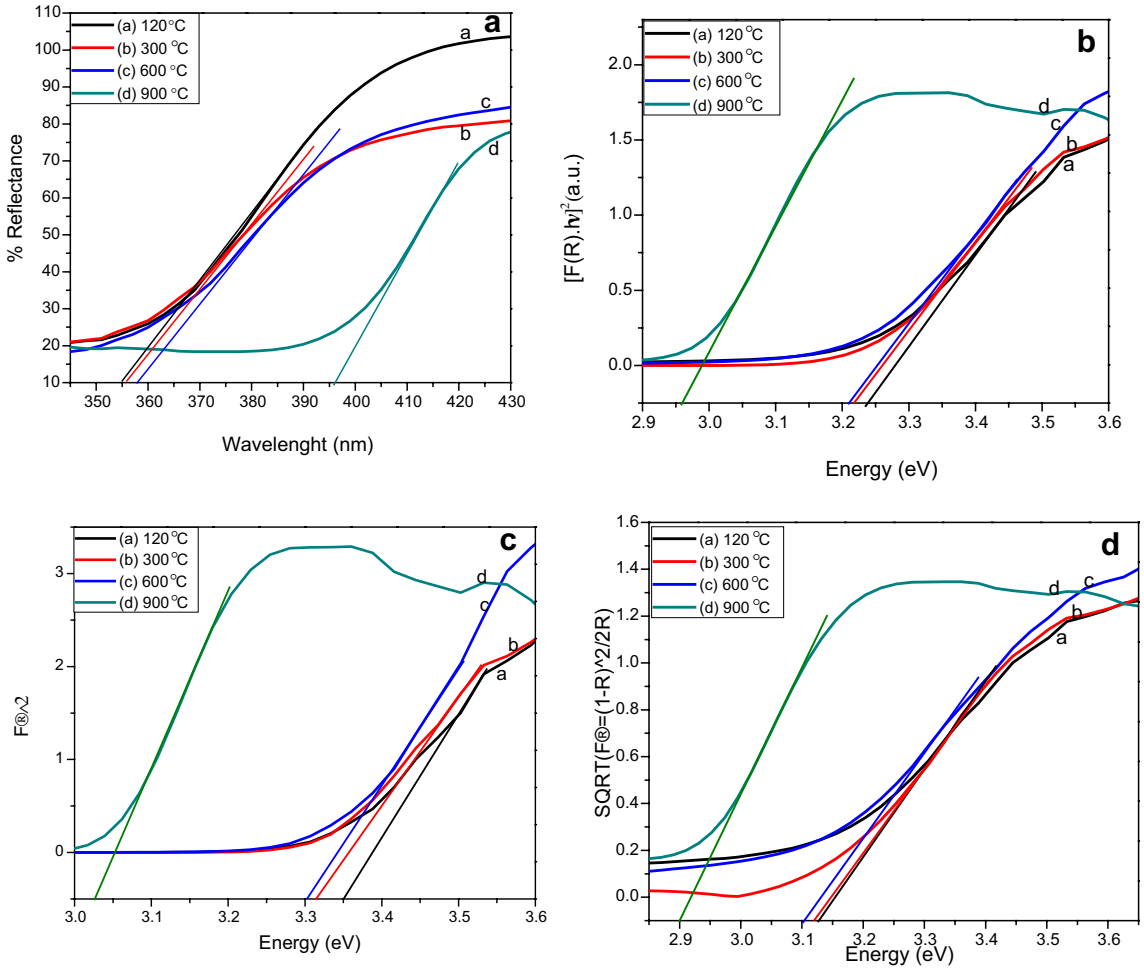

Fig. 4 DRS spectra (**a**), Kubelka Monk Spectra (**b**), Direct Band gap Spectra (**c**) and indirect band gap spectra (**d**) of TiO_2 nanoparticles heated at different temperatures

Table 4 Band gap energy of TiO_2 nanoparticles calculated by different methods

Temperature (°C)	Transmittance edge	Direct spectrum band gap	Kubelka monk band gap	Direct band gap	Indirect band gap
120	354.78	3.49	3.23	3.34	3.12
300	356.05	3.48	3.21	3.31	3.11
600	358.03	3.46	3.20	3.30	3.10
900	396.10	3.13	2.95	3.02	2.89

may be explained on the basis of oxygen release on the surface of TiO_2 nanoparticles, generating hydrogen peroxide after the reaction of TiO_2 suspension with water. The generation of H_2O_2 strongly depends on the small size and large surface area of the TiO_2 particles having more oxygen on the surface. The H_2O_2 can, therefore, penetrate to cell membrane and cause fetal damage to bacterial cell as suggested in previous findings (Sunada et al. 1998; Fang et al. 2006).

Conclusion

The TiO_2 nanoparticle was synthesized by chemical precipitation method and heated till 900 °C after the transformation of phase above 600 °C. It was found that the crystallite and pore sizes increase with increasing heating temperature while surface area, pore volume, lattice strain and dissolution density decreases. The band gap energies of TiO_2 nanoparticles at different temperatures were calculated by applying different methods which decrease at

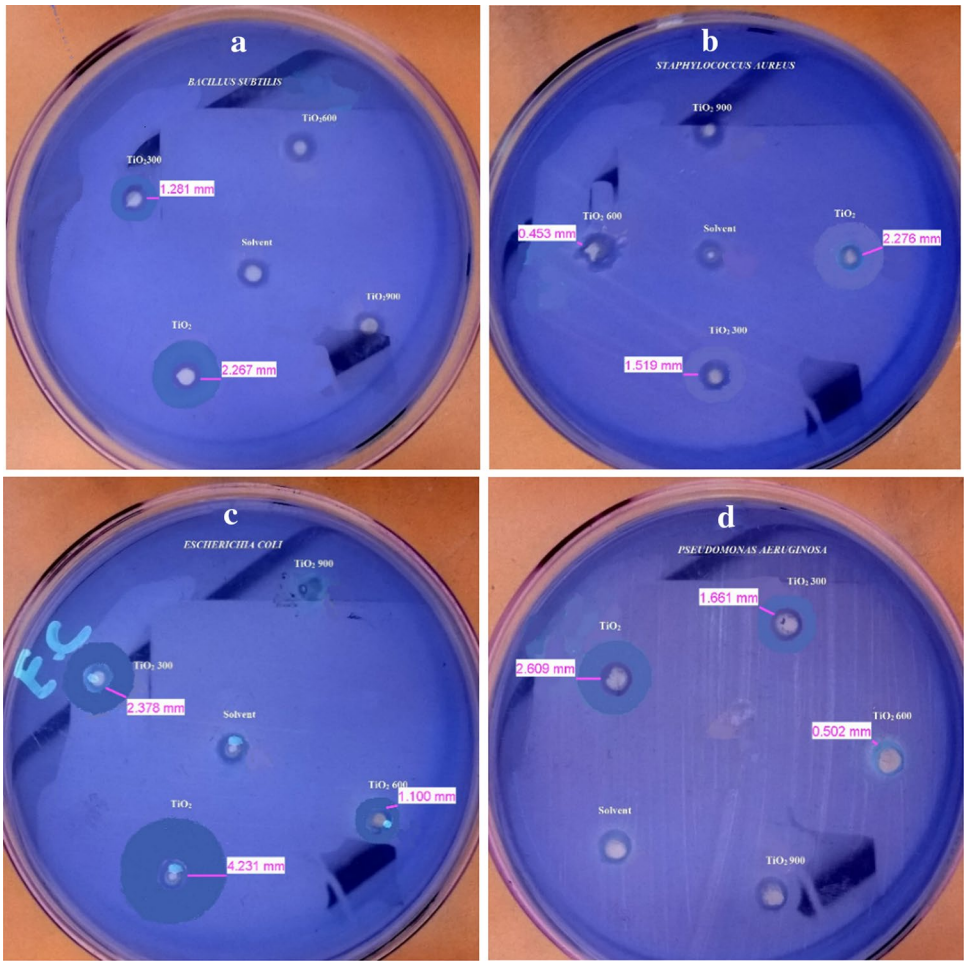

Fig. 5 Antibacterial activity for B subtilis (**a**), S aureus (**b**), *E. Coli*, (**c**) and P aeruginosa (**d**)

Table 5 Inhibition zones measure in (mm) for TiO_2 nanoparticles against bacterial strain

Bacterial species	120 °C	300 °C	600 °C	900 °C	Solvent
B. subtilis	2.267	1.281	–	–	–
S. aureus	2.276	1.519	0.453	–	–
E. coli	4.231	2.378	1.100	–	–

elevating temperatures. The antibacterial activity of particles was significantly decreased with increasing the heating temperature. The large size and small surface area of the nanoparticles may be the reason for having limited number of oxygen atoms to generate H_2O_2.

Methods

Materials

Analytical grade titanium isopropoxide and ethanol were purchased from Sigma Aldrich and were used as received.

Synthesis of TiO_2 nanoparticles

In typical synthesis, 1.7 mL of titanium isopropoxide was added to 70 mL of deionized water with constant stirring for 15 min and then 30 mL ethanol was added to this homogenized solution. The solution was further stirred and heated for 90 min at 55 °C and was suddenly cooled down to room temperature. The particles thus appeared were filter and heat treated at 120, 300, 600 and 900 °C using muffle furnace for 3 h and stored in polyethylene bottles for further study.

Characterization of TiO_2 nanoparticles

The structural and morphological characterization of TiO_2 nanoparticles were performed by X-ray diffraction model Panalytical X-Pert Pro. The source for X-ray generation was Cu (1.54 Å) at 40 kV voltage and the current was 30 mA. The surface area, pore volume and pore size of TiO_2 nanoparticles heated at temperature were measured by N_2 adsorption using single point and multipoint BET surface areas, Langmuir Plot, t-Plot and BJH cumulative methods. The FTIR spectra of the samples were recorded

on FTIR spectrophotometer model Nicolet 560 in the range 500–4000 cm^{-1}. The thermal (TG/DTG) analysis of the samples was performed by Perkin Elmer Model 6300 TG/DTA analyzer. A known quantity of the samples was heated to 1000 °C, starting from 40 °C with heating rate 10 °C/min under air atmosphere. The optical property of TiO_2 nanoparticles was studied by UV visible absorbance spectroscopy (diffuse reflectance spectroscopy (DRS) UV–VIS/NIR spectrometer lambda 950 with integrating sphere of 200–2500 nm.

Bioactivity assay

A well-known agar well diffusion method was used to screen TiO_2 nanoparticles heated at different temperature against gram-positive and gram-negative bacteria using agar nutrient as medium (Bauer et al. 1966). For antimicrobial disk diffusion susceptibility test, 0.5 McFarland solution was used for clinical strain where microorganism on media were streaked with the help of sterile swabs. Then stock suspension was prepared by dispersing 1 mg of TiO_2 heated at different temperature in 1 mL of normal saline. 100 µL of each suspension was added to each well in plates and were incubated in incubator at 37 °C. The inhibition zone was measured after 24 h and taken as the activity of the TiO_2 nanoparticles against examine bacteria.

References

Arami H, Mazloumi M, Khalifehzadeh R, Sadrnezhaad SK (2007) Sonochemical preparation of TiO_2 nanoparticles. Mater Lett 61:4559–4561

Bauer AW, Kirby WM, Sherris JC, Turck M (1966) Antibiotic susceptibility testing by a standardized single disk method. Am J Clin Pathol 45(4):493–496

Chen YF, Lee CY, Yeng MY, Chiu HT (2003) The effect of calcination temperature on the crystallinity of TiO_2 nanopowders. J Cryst Growth 247(3):363–370

Cheng H, Ma J, Zhao Z, Qi L (1995) Hydrothermal preparation of uniform nanosize rutile and anatase particles. Chem Mater 7(4):663–671

Dai Y, Cobley CM, Zeng J, Sun Y, Xia Y (2009) Synthesis of anatase TiO_2 Nanocrystals with exposed 001 facets. Nano Lett 9:2455–2459

Durand SP, Rouviere J, Guizard C (1995) Sol–gel processing of titania using reverse micellar systems as reaction media. Colloids Surf A 98:251–270

Durucan C, Akkopru B (2010) Effect of calcination on microstructure and antibacterial activity of silver-containing silica coating. Wiley Inter Sci 93:448–454

Fang M, Chen JH, Xu XL, Yang PH, Hildebrand HF (2006) Antibacterial activities of inorganic agents on six bacteria associated with oral infections by two susceptibility tests. Int J Antimicrob Agents 27(6):513–517

Farrukh MA, Tan P, Adnan R (2012) Influence of reaction parameters on the synthesis of surfactant-assisted tin oxide nanoparticles. Turk J Chem 36:303–314

Gaber A, Abdel- Rahim MA, Abdel-Latief AY, Abdel-Salam MN (2014) Influence of calcination temperature on the structure and porosity of nanocrystalline SnO_2 synthesized by a conventional precipitation method. Int J Electrochem Sci 9:81–95

Gao X, Cui Y, Levenson RM, Chung LW, Nie S (2004) In vivo cancer targeting and imaging with semiconductor quantum dots. Nat Biotechnol 22(8):969–976

Han X, Kuang Q, Jin M, Xie Z, Zheng L (2009) Synthesis of Titania nanosheets with a high percentage of exposed (001) facets and related photocatalytic properties. J Am Chem Soc 131:3152–3153

Joo J, Kwon SG, Yu T, Cho M, Lee J, Yoon J, Hyeon T (2005) Large-scale synthesis of TiO_2 nanorods via nonhydrolytic SolGel ester elimination reaction and their application to photocatalytic inactivation of *E. coli*. J Phys Chem B 109:15297–15302

Kayani ZN, Saleemi F, Batool I (2015) Effect of calcination temperature on the properties of ZnO nanoparticles. Appl Phys A 119(2):713–729

Kim EJ, Hahn SH (2001) Microstructural changes of microemulsion-mediated TiO_2 particles during calcination. Mater Lett 49(3):244–249

Kumar KN, Keizer K, Burggraaf AJ (1993) Textural evolution and phase transformation in titania membranes: part 1.—Unsupported membranes. J Mater Chem 3(11):1141–1149

Li J, Wang LW (2003) Shape effects on electronic states of nanocrystals. Nano Lett 3:1357–1363

Mazdiyasni KS, Lynch CT, Smith JS (1965) Preparation of ultrahigh-purity submicron refractory oxides. J Am Ceram Soc 48(7):372–375

Nagarani N (2013) Structural and optical characterization of ZnO thin films by sol–gel method. J Photo Spint 2:2324–8572

Padmavathy N, Vijayaraghavan R (2008) Enhanced bioactivity of ZnO nanoparticles—an antimicrobial study. Sci Technol Adv Mater 9:035004. 7 pp

Paunesku T, Rajh T, Wiederrecht G, Maser J, Vogt S, Stojicevic N, Protic M, Lai B, Oryhon J, Thurnauer M, Woloschak G (2003) Biology of TiO_2-oligonucleotide nanocomposites. Nat Mater 2:343–346

Prasad TNVKV, Elumalai EK, Khateeja S (2011) Evaluation of the antimicrobial efficacy of phytogenic silver nanoparticles. Asian Pac J Trop Biomed 1(1):82–85

Samuneva B, Kozhukharqv V, Trapalis C, Kranold R (1993) Sol–gel processing of titanium-containing thin coatings. J Mater Sci 28:2353–2360

Sun L, Qin Y, Cao Q, Hu B, Huang Z, Ye L, Tang X (2011) Novel photocatalytic antibacterial activity of TiO_2 microspheres exposing 100% reactive 111 facets. Chem Commun 47:12628–12630

Sunada K, Kikuchi Y, Hashimoto K, Fujishima A (1998) Bactericidal and detoxification effects of TiO_2 thin film photocatalysts. Environ Sci Technol 32(5):726–768

Uddin MT, Nicolas Y, Olivier C, Toupance T, Servant L, Müller MM, Kleebe HJ, Ziegler J, Jaegermann W (2012) Nanostructured SnO_2–ZnO heterojunction photocatalysts showing enhanced photocatalytic activity for the degradation of organic dyes. Inorg Chem 51(14):7764–7773

Van den Bogaard AE, Stobberingh EE (2000) Epidemiology of resistance to antibiotics. Links between animals and humans. Int J Antimicrob Agents 14:327–350

Verdier T, Coutand M, Bertron A, Roques C (2014) Antibacterial activity of TiO_2 photocatalyst alone or in coatings on *E. coli*: the influence of methodological aspects. Coatings 4(3):670–686

Wang R, Hashimoto K, Fujishima A, Chikuni M, Kojima E, Kitamura A, Shimohigoshi M, Watanabe T (1997) Light-induced amphiphilic surfaces. Nature 388:431–432

Wang XS, Wu ZC, Webb JF, Liu ZG (2003) Ferroelectric and dielectric properties of Li-doped ZnO thin films prepared by pulsed laser deposition. Appl Phys A 77:561–569

Waseem M, Mustafa S, Naeem A, Koper GJ, Shah KH (2011) Cd^{2+} sorption characteristics of iron coated silica. Desalination 277(1):221–226

West AR (1986) Solid state chemistry and its applications. Wiley, New York, p 174

Yang HG, Sun CH, Qiao SZ, Zou J, Liu G, Smith SC, Cheng HM, Lu GQ (2008) Anatase TiO_2 single crystals with a large percentage of reactive facets. Nature 453:638–641

Yang H, Liu G, Qiao S, Sun C, Jin Y, Smith SC, Zou J, Cheng HM, Lu GQ (2009) Solvothermal synthesis and photoreactivity of anatase TiO_2 Nanosheets with dominant 001 Facets. J Am Chem Soc 131:4078–4083

Yu JG, Yu HG, Cheng B, Zhao XJ, Yu JC, Ho WK (2003) The effect of calcination temperature on the surface microstructure and photocatalytic activity of TiO_2 thin films prepared by liquid phase deposition. J Phys Chem B 107(50):13871–13879

Zhao X, Quan X, Chen S, Zhao H, Liu YJ (2007) Photocatalytic remediation of γ-hexachlorocyclohexane contaminated soils using TiO_2 and montmorillonite composite photocatalyst. J Environ Sci 19:358–361